CELL SCALE ELECTROPERMEABILIZATION MODELING

We present a new model of *in vitro* cell electropermeabilization, which describes separately the conducting state and the permeable state of the membrane submitted to high voltage pulses. We first derive the model based on the experimental observations and we present the numerical methods to solve the non-linear partial differential equations. We then present numerical simulations that corroborate qualitatively the experimental data dealing with the uptake of fluorescent dyes after millipulses. This tends to justify the validity of our modeling. Forthcoming work will be to calibrate the parameters of the model for quantitative description of the uptake.

Michael LEGUÈBE[1], Aude SILVE[2], Clair POIGNARD[1] and Lluis M MIR[3].

1. INRIA Project team MC2, Institut de Mathématiques de Bordeaux, Université de Bordeaux.
2. Institute for Pulse Power and Microwave Technology, Karlsruhe Institute of Technology.
3. Institut Gustave Roussy, Laboratoire de Vectorologie et Thérapeutiques Anticancéreuses.

Model statement

- Experiment #1, Escoffre *et al.* [1] : propidium iodide (PI) uptake by a cell submitted to 10 pulses of 20 ms, 50 kV/m, 1 Hz. A dyssymetry in the PI distribution can be seen, facing the anode (lower part on the picture). PI internalization lasts for several seconds after pulses.

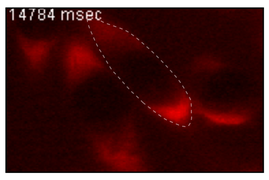

- Experiment #2, Benz *et al.* [2] : voltage during the discharge of a planar membrane previsouly charged with electric fields of various magnitudes. After only 5 µs, the membrane conductivity stabilizes at a value close to its original state.

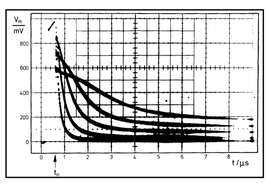

- Experiment #3, Silve *et al.* : *in vitro* cells are submitted to a single pulse of 100 µs, 150 kV/m. A cytotoxic agent (bleomycin) is injected after the pulses. We notice clearly an effect of bleomycin even if it is injected ten minutes after the pulse application.

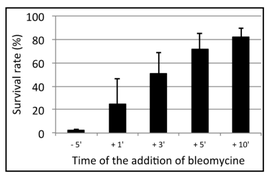

- Experiments #1 and #3, as well as a majority of electroporation experiments, are based on the internalization of a given molecule by the cell. We should not restrict our study on the electrical properties of the cell, like existing models, but also include a model of transport and diffusion of molecules. Heavy molecules, such as DNA plasmids, are carried towards the cell by electrophoresis only, whereas smaller molecules can diffuse in both extra- and intracellular media.

- Experiments #2 and #3 highlight two distinct dynamics of the cell recovery to its initial state. The conducting state of the membrane lasts for microseconds, while its permeable state lasts for several minutes. Thus we cannot characterize cell permeability by its membrane conductivity. The phenomenon would be the following:

1./ Membrane at rest

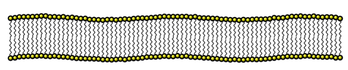

2./ During the pulse : conductive pores creation. Lipids are chemically altered.

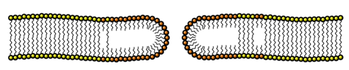

3./ Few microseconds after the pulse: pores now closed, permeable membrane.

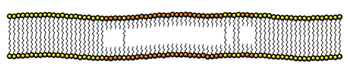

4./ Diffusion of altered lipids, membrane reconstruction by exocytosis.

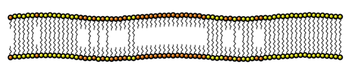

- Media O_e and O_i are considered homogeneous, and the membrane Γ is a single interface. The electric potential U follows a Poisson's law, and the concentration of a molecule M is governed by a transport-diffusion equation. In $O_e \cup O_i$:

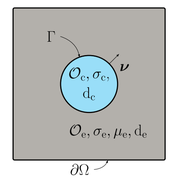

$$\Delta U = 0, \qquad \partial_t M - d\Delta M = 0,$$

with the transmission conditions on the flux and discontinuities on Γ:

$$\begin{cases} \sigma_e \partial_\nu U^e = \sigma_c \partial_\nu U^c, \\ C_m \partial_t [U] + S_m(t,[U])[U] = \partial_\nu U^c, \end{cases} \quad \begin{cases} d_e \partial_\nu M^e + \mu_e M^e \partial_\nu U^e = d_c \partial_\nu M^c, \\ P_m(t,[U])[M] = d_c \partial_\nu M^c, \end{cases}$$

with the following boundary and initial conditions

$$\begin{cases} U(t,\cdot)|_{\partial\Omega} = U_{imp}(t,\cdot), \\ U(0,\cdot) = U_0. \end{cases} \quad \begin{cases} M(t,\cdot)|_{\partial\Omega} = M^0, \\ M(0,\cdot) = M^0 \mathbb{1}_{\mathcal{O}_e}. \end{cases}$$

- The non-linear terms S_m and P_m denote respectively the surface conductivity and the permeability of the membrane. We note (S_0,S_1,S_2) and (P_0,P_1,P_2) the conductivities and permeabilities of the membrane at rest, completely porous, and completely altered.

$$S_m(t,s) = S_0 + X_1(t,s) S_1 + X_2(t,s) S_2, \quad \forall t > 0, s \in \Gamma,$$
$$P_m(t,s) = P_0 + X_1(t,s) P_1 + X_2(t,s) P_2, \quad \forall t > 0, s \in \Gamma.$$

- X_1 and X_2 describe respectively the membrane porosity and permeability degrees ($0<X_1,X_2<1$). X_1 follows an electrophysiology sliding-door model and is triggered by a voltage threshold, represented by a smoothed Heaviside function β_1:

$$\begin{cases} \partial_t X_1 = \dfrac{\beta_1([U]) - X_1}{\tau_1}, \\ X_1(t=0,s) = X_1^0, \end{cases} \quad \text{with } \beta_1(\lambda) = \frac{1 + \tanh(k_1(|\lambda| - V_{th}))}{2}.$$

X_2 follows a reaction-diffusion equation, with different dynamics of permeabilization and recovery ($\tau_{2,perm}$~5µs, but $\tau_{2,res}$~1h). X_2 grows as soon as a porosity threshold is passed.

$$\begin{cases} \partial_t X_2 - d_L \Delta_\Gamma X_2 = \dfrac{\beta_2(X_1) - X_2}{\tau_{2,perm}} \text{ if } \beta_2 - X_2 > 0, \\ \partial_t X_2 - d_L \Delta_\Gamma X_2 = \dfrac{\beta_2(X_1) - X_2}{\tau_{2,res}} \text{ if } \beta_2 - X_2 < 0, \\ X_2(t=0,s) = X_2^0, \end{cases}$$
$$\beta_2(\lambda) = \frac{1 + \tanh(k_2(|\lambda| - X_{1,th}))}{2}.$$

Numerical methods

Discretization of electric potential and molecule transport equations

- A 3D parallel code has been written to simulate our permeabilization model. It is based on a second order finite differences method proposed by Cisternino and Weynans [3], whose main feature is to add unknowns at the intersection points of a cartesian grid and the interface Γ. Two examples of Laplacian and interface fluxes discretization stencils are given below in 2D. Those special stencils allow a second order convergence for the linear problem (constant S_m), and a first order convergence for the non-linear problem.

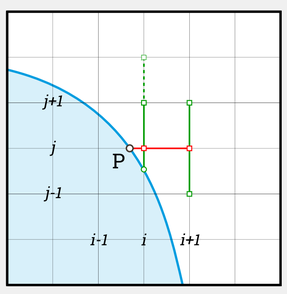

◀ Example of flux discretization at interface point P, located left from *ij* :

$$\partial_\nu U(P) = \nabla U(P) \cdot \nu(P) = \partial_x U(P) \nu_x(P) + \partial_y U(P) \nu_y(P).$$

The *x*-derivative is discretized with the red points, whereas the *y*-derivative is approximated by a linear combination of the derivatives at points *ij* and *i+1j*. If the *y*-derivative at point *ij* involves another interface point, the stencil is shifted (dotted line).

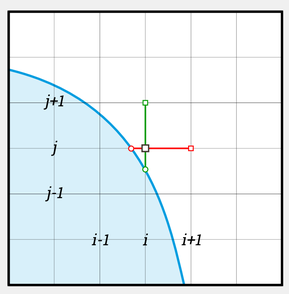

Laplacian discretization stencil near the interface. ▶

- Numerical schemes : our very irregular mesh induces numerical instabilities for the transport-diffusion equation on *M*. Thus, a splitting of these two steps is performed. A fixed point method is performed for the diffusion step to capture accuratly the non-linearity of P_m.

$$\begin{cases} (\Delta u)^{n+1} = 0, \\ \sigma_c (\partial_\nu u^c)^{n+1} - \sigma_e (\partial_\nu u^e)^{n+1} = 0, \\ \left(\dfrac{C_m}{\delta t} - S_m{}^n \right) [U]^{n+1} - \sigma_e (\partial_\nu u^e)^{n+1} = \dfrac{C_m}{\delta t} [U]^n. \end{cases}$$

$$\begin{cases} \dfrac{1}{\delta t} M^* = \dfrac{1}{\delta t} M^n + (\nabla \cdot (\mu M \nabla u))^n, \\ \partial_\nu M^* = 0 \text{ if } \nabla u^n \cdot \nu > 0 \text{ on } \Gamma, \\ M^* = 0 \text{ if } \nabla u^n \cdot \nu < 0 \text{ on } \Gamma. \end{cases} \quad \begin{cases} \dfrac{1}{\delta t} M^{k+1} - d(\Delta M)^{k+1} = \dfrac{1}{\delta t} M^k, \\ d_e (\partial_\nu \mu_e)^{k+1} - d_c (\partial_\nu \mu_c)^{k+1} = \mu_e M_j^{e,*} (\partial_\nu u_e)^n, \\ P_m (M^{e,k+1} - M^{c,k}) = d_e (\partial_\nu \mu_e)^{k+1}, \\ \text{while } \left\| M^{k+1} - M^k \right\|_{L^2(\Omega)} > 10^{-6}. \end{cases}$$

Discretization of the Laplace-Beltrami Operator (LBO) on the interface

- The equation on X_2 includes diffusion on the surface Γ. We studied the convergence of a finite volumes based method [4] to discretize the LBO, with the intersection points previously used (mesh A), as well as a more regular mesh of a sphere(B). Since the results are not staisfying and the cell shapes usually simple, we use directly the analytical expression of the LBO thanks to a parametrization in (θ,φ) of Γ:

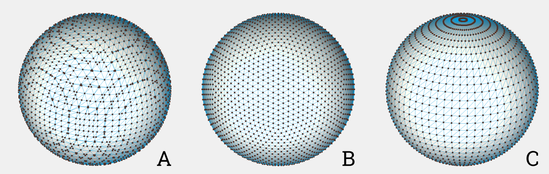

▲ Sphere meshes used to select a LBO discretization method.

$$g_{\theta\theta} := |\partial_\theta \Gamma(\theta,\varphi)|_2^2, \quad g_{\varphi\varphi} := |\partial_\varphi \Gamma(\theta,\varphi)|_2^2, \quad g_{\theta\varphi} := \langle \partial_\theta \Gamma(\theta,\varphi), \partial_\varphi \Gamma(\theta,\varphi) \rangle.$$
$$\mathcal{G} := \begin{pmatrix} g_{\theta\theta} & g_{\theta\varphi} \\ g_{\theta\varphi} & g_{\varphi\varphi} \end{pmatrix}, \quad g := \det(\mathcal{G}), \quad \mathcal{G}^{-1} := \begin{pmatrix} g^{\theta\theta} & g^{\theta\varphi} \\ g^{\theta\varphi} & g^{\varphi\varphi} \end{pmatrix}.$$
$$\Delta_\Gamma f(\theta,\varphi) = \frac{1}{\sqrt{|g|}} \left[\partial_\theta \left(\sqrt{|g|} \left(g^{\theta\theta} \partial_\theta f + g^{\theta\varphi} \partial_\varphi f \right) \right) + \partial_\varphi \left(\sqrt{|g|} \left(g^{\theta\varphi} \partial_\theta f + g^{\varphi\varphi} \partial_\varphi f \right) \right) \right].$$

The LBO is then discretized using a standard second order centered finite differences method on a cartesian grid in (θ,φ) (mesh C). A correction must be done at the poles where the metric $\mathcal{G}$ is not defined.

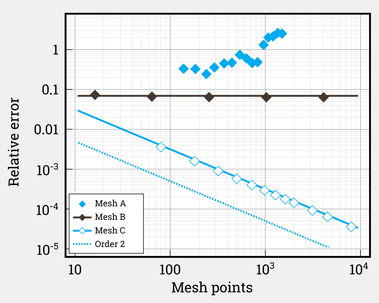

◀ Convergence (or not) in L^∞ norm of the finite volumes methods on meshes A and B and finite differences method on mesh C. The relative error is measured by computing the curvature $\boldsymbol{H}=\Delta_\Gamma \Gamma$ of the sphere.

Spatial repartition of the relative error when computing the curvature of an ellipsoid. The error is maximal at the poles, where $\sin\theta = 0$. ▶

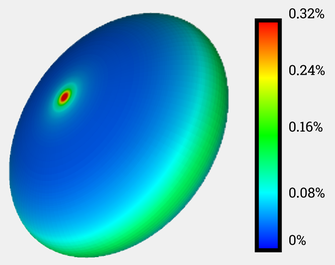

Simulations

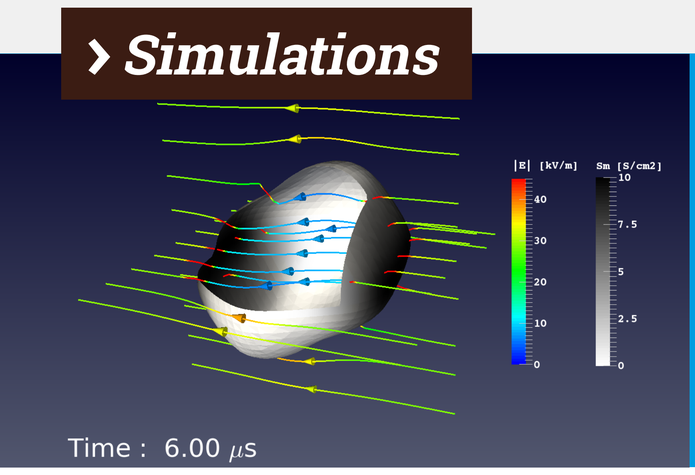

◀ Electric field and conductivity of the cell membrane submitted to a pulse of 100 µs, 40 kV/m.

2D Simulation of PI transport around and inside a cell similarly shaped as the cell shown in experiment #1, submitted to the same pulse protocol as the experiment. The color scales are not the same since there is a important gap between the values in the two subdomains. The lipid diffusion is not taken into account in this result. ▶

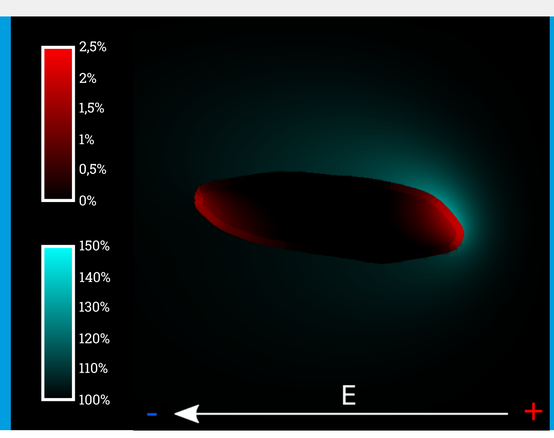

2D Simulation of PI transport (without lipid diffusion) for a cell submitted to the same pulse protocol as used by Vernier *et al.* in [5] : five pulses of 100 µs, 500 kV/m, 4Hz. The indicated times start at the end of the last pulse. Same color scale as to the left. ▶

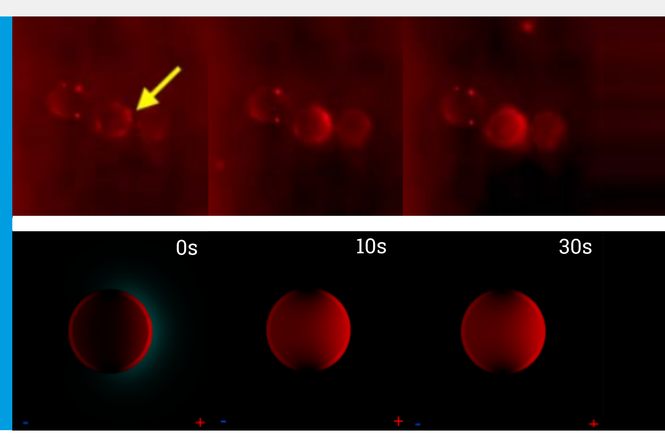

Influence of pulse frequency on global permeabilization

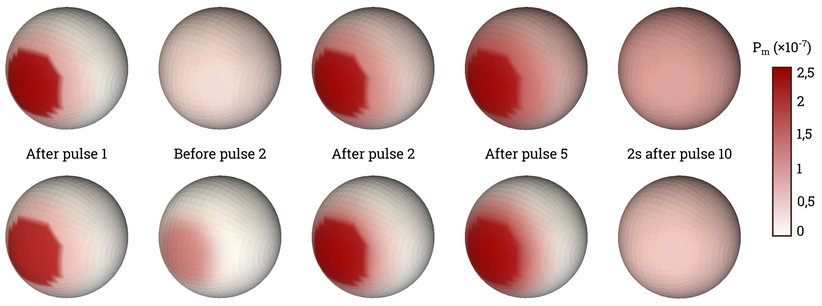

Permeabilization P_m of a cell submitted to 10 pulses of 40kV/m ▲ during 10 µs. The top line corresponds to a time lapse of 1s between pulses and 1ms for the bottom line.

- When the duration between two electric pulses is small, the lipids don't have the time to spread evenly on the membrane surface. When the next pulses occur, the same region is porated, and the total quantity of altered lipids is higher when the pulse frequency is lower. This result corroborate those recently obtained by Silve *et al.* [6], highlighting this "desensitization" effect of high-frequency pulses.

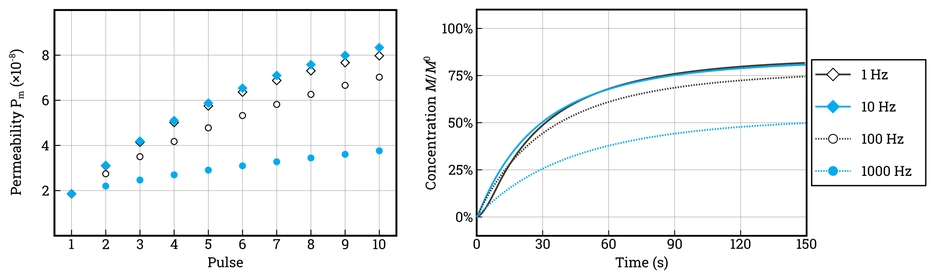

▲ Averaged permeabilization degree P_m after each pulse (left panel) and time evolution of the molecule concentration *M* (right panel), relatively to the external concentration M^0, for pulse application frequency from 1 to 1000 Hz.

References

- [1] J.M. Escoffre, T. Portet, C. Favard, J. Teissié, D. Dean, and M.P. Rols. *Electromediated formation of DNA complexes with cell membranes and its consequences for gene delivery.* BBA - Biomembranes, 1808(6), 2011.
- [2] R. Benz, F. Beckers, and U. Zimmermann. *Reversible electrical breakdown of lipid bilayer membranes: a charge pulse relaxation study.* J. Memb. Biol., 48(2), 1979.
- [3] M. Cisternino and L. Weynans. *A parallel second order cartesian method for elliptic interface problems.* Commun. Comput. Phys. 12, 2012
- [4] G. Xu. *Discrete Laplace–Beltrami operators and their convergence.* Comput. Aided Geom. Des., 21(8), 2004.
- [5] T. Vernier, Y. Sun, L. Marcu, S. Salemi, C.M. Craft, and M.A. Gundersen. *Calcium bursts induced by nanosecond electric pulses.* Biochem. Biophys. Res. Comm., 310 (2), 2003.
- [6] A. Silve, A. Giumerà Brunet, A. Ivorra, and L.M. Mir. *Comparison of the effects of the repetition rate between microsecond and nanosecond pulses: Electropermeabilisation-induced electro-desensitization?* Submitted, 2014.

More information

- M. Leguèbe, A. Silve, C. Poignard and L.M. Mir. *Conducting and permeable states of cell membrane sbmitted to high voltage pulses. Mathematical and numerical studies based on experiments.* Submitted, 2014.
- O. Kavian, M. Leguèbe, C. Poignard, and L. Weynans. *"Classical" electropermeabilization modeling at the cell scale.* J. Math. Biol., 68(1–2), 2014.
- M. Leguèbe, C. Poignard, and L. Weynans. *A second-order cartesian method for the simulation of electropermeabilization cell models.* Research report RR-8302, INRIA, 2013.

This study has been carried out in the frame of "the Investments for the future" Programme IdEx Bordeaux CPU (ANR-10-IDEX-03-02). The authors have been partly granted by the French national agency throughout the research projects INTCELL (2010–BLAN–916–04) and MEMOVE (2011–BS01–006–01). This work was partly performed in the scope of the European Associated Laboratory EBAM.